SECOND REVISED VERSION

Full torso and limited-domain computer models for epicardial pulsed electric field ablation

Ana González-Suárez[1,2*], Ramiro M. Irastorza[3,4], Stuart Deane[5], Barry O'Brien[5], Martin O'Halloran[1,2], Adnan Elahi[1,2]

[1]*Electrical and Electronic Engineering, National University of Ireland Galway, Ireland,*

[2]*Translational Medical Device Lab, National University of Ireland Galway, Ireland,*

[3] *Instituto de Física de Líquidos y Sistemas Biológicos (CONICET), La Plata, Argentina*

[4] *Departamento de Ingeniería Mecánica, Universidad Tecnológica Nacional, Facultad Regional La Plata, La Plata, Argentina*

[5] *AtriAN Medical Limited, Unit 204, NUIG Business Innovation Centre, Upper Newcastle, Galway, Ireland*

***Corresponding author:** Dr. Ana González-Suárez, Translational Medical Device Lab, 2nd Floor, Lambe Translational Research Facility, University College Hospital Galway, Ireland. Email: ana.gonzalezsuarez@nuigalway.ie

Word count: 5,545

Running head: Computer modeling for epicardial pulsed electric field ablation

Abstract

Background and objectives: Pulsed Electric Field (PEF) ablation has been proposed as a non-thermal energy to treat atrial fibrillation (AF) by ablation of ganglionated plexi using the epicardial approach. The electric field distribution at the target site (heart) and its surroundings has not yet been assessed previously, using epicardial ablation technique. Our objective was to develop computational models, incorporating the real anatomy of the heart and the patient's torso, to assess the electric field distribution when applying epicardial monopolar PEF.

Methods: A novel 3D realistic full torso model was built with the multi-electrode ablation device placed on the epicardium and a dispersive pad on the patient's back to evaluate the electric field distribution. The 400 V/cm isoline was used to estimate the 'PEF-zone'. A 3D limited-domain model was also built including only the region of interest around the ablation device to assess its validity in comparison with the full torso model.

Results: The electrical field is mainly limited to the target site (PEF-zone with lengths of 25.79 to 29.00 mm, depths of 5.98–7.02 mm and maximum widths of 8.75–10.57 mm) and is practically negligible in adjacent organs (<30 V/cm and <36 V/cm in oesophagus and lungs, respectively). The electrical currents ranged from 3.67 A to 7.44 A. The 3D limited-domain model provided a similar electric field distribution to those obtained from the 3D full torso models (differences < 0.5 mm in PEF-zone depth).

Conclusions: Computational results suggest that PEF-zone is very focused around the ablation catheter. Limited-domain models offer similar results in terms of PEF-zone size, reducing the complexity of the modelling.

Key words: Cardiac arrhythmia; computer modelling; epicardial ablation; limited-domain model; pulsed field ablation; torso model.

1. Introduction

High-intensity Pulsed Electric Field (PEF) ablation, also known as Pulsed Field Ablation (PFA), has been proposed as a non-thermal energy to ablate cardiac tissue with the intended purpose to cure arrhythmias. This energy provokes permeabilization of the cell membrane (creation of pores), leading to cellular homeostasis disruption and cell death [1]. It is currently a very promising ablation technique, particularly for pulmonary vein isolation [2,3]. PEF ablation has also been recently proposed to ablate cardiac ganglionic plexi (GP) since the contribution of the autonomic nervous system to the induction and maintenance of atrial fibrillation (AF) is increasingly appreciated [4]. The purpose of this technique is to destroy GPs, which are embedded in epicardial fat [5–7]. While the epicardial approach is assumed to directly deliver PEF energy to the target site, it is nevertheless important to assess if the electric field might also affect other organs in the vicinity (such as lungs and oesophagus).

Computer modelling has been broadly used to study ablative techniques to treat AF [8,9]. Although computational models have been developed to study PEF in the context of tumour [10] and endocardial [11,12] ablation, no computer model has been previously developed for epicardial ablation aimed at destroying GPs. In this context, we modelled a multi-electrode epicardial device (AtriAN Medical, Galway, Ireland) designed to treat AF by means of applying high voltage pulses to the ganglionated plexi. The device comprises four metal electrodes, each having a hole through which saline is infused (see Fig. 1C). The

thin layer of saline between the electrodes of the device and the heart acts as a ‘virtual electrode’, thereby ensuring the transmission of electrical energy to the target and preventing damage to the surrounding structures [5]. Our objective was to develop computational models incorporating the real anatomy of the heart and the full torso of the patient for the assessment of the electric field distribution on the target zone and its surroundings upon application of the pulsed voltage. Additionally, we assessed whether a limited-domain model (i.e. not considering the entire torso but only a tissue fragment around the device) could offer similar results to that of the complete torso, thus reducing complexity and computational cost.

2. Methods

2.1. Full torso model geometry

A three-dimensional realistic model was built based on the full torso of a patient. This model considered an entire patient’s torso with a standard dispersive pad placed on its back, a complete heart structure, and adjacent organs (lungs and oesophagus) (Fig. 1A). To be more precise, the three-dimensional model was built on the basis of files from the Virtual Population V2.0, specifically those from a 34-year old male (Duke) [13]. This human model consists of 22 files in stl format obtained using Whole-body Magnetic Resonance Imaging (WB-MRI) according to a protocol presented in [13]. We used three of the 22 files that detail the non-intersecting surfaces of different tissues and organs: Heart.stl, Respiratory_system.stl, and Other_tissue.stl, from which (after properly cutting and selecting) we extracted the external surfaces of the heart, the lungs, oesophagus and the torso, respectively. The procedure of mesh trimming and simplifying

was carried out using MeshLab Visual Computing Lab software (http: //meshlab.sourceforgel.net) [14]. Surfaces were imported into the meshing software Gmsh [15] and used to create and remesh the respective volumes with ad hoc Python scripts and the routines described in [16]. The rest of the torso was considered to be a homogeneous medium. The dimensions of the ablation device modeled were the same as the real device: 3.98 mm diameter, four metal electrodes of 3.18 mm length separated by a distance of 3.05 mm and a 0.76 mm diameter irrigation hole in the centre of each electrode. The metal electrodes of the ablation device were assumed to be in direct contact with the epicardial surface, as is shown in Figure 1B. The dispersive pad was modelled as an electrical rectangular surface boundary condition of 180 mm x 115 mm (corresponding to the real surface of a dispersive pad) on the back of the patient's torso.

2.2. Limited-domain model geometry

We assessed the possibilities of a 3D limited-domain model to predict the PEF-zone size, i.e. a model which only considers a fragment of the region of interest around the ablation device (specifically a fragment of the heart and patient's torso). We compared the electric field distributions computed with this model to those obtained with the full torso model. The limited-domain model is much easier to build than the full torso model, and could allow studying in the future specific issues related with epicardial PEF ablation by including more realistic details, such as the characteristics of the thin saline layer, heterogeneity of the myocardial wall, etc. Figure 2 shows the geometry of the 3D limited-domain model, which includes adjacent organs located in the proximity to the target zone (oesophagus and lungs) and connective tissue between the organs. The oesophagus was

assumed to be collapsed with 3 mm wall thickness, 0.1 mm lumen filled with saliva, and having a length of 30 mm [17]. The connective tissue layer was of 1 mm placed between the back of the ablation device and the oesophagus. The outer dimensions were similar to those of limited-domain models of cardiac radiofrequency ablation, specifically X = 80 mm and Z = Y = 40 mm [18], with distance from the ablation device to the dispersive pad of 45 mm. We checked that these outer dimensions were suitable by a sensitivity analysis (more details in 3.3 Section of Results).

2.3. Governing equations

The model was based on an electrical problem, which was solved numerically by the Finite Element Method (FEM) with COMSOL Multiphysics (COMSOL, Burlington, MA, USA). The meshing for the 3D full torso model had more than twice as many tetrahedral elements as the 3D limited-domain model (~300,000 for the full torso vs. ~110,000 for the limited-domain model). The 'quasi-statics/electric' application mode of AC/DC module of COMSOL [19] was employed to compute the electric field distribution when a voltage pulse of 1000 V was applied between the ablation electrodes and the dispersive pad. The transient cellular responses were not considered (i.e. membrane charging), then the electric field distribution can be computed by solving Maxwell's equations in its Laplacian form [1]:

$$\nabla(\sigma\nabla\phi) = 0 \quad (1)$$

$$\boldsymbol{E} = -\nabla\phi \quad (2)$$

$$\boldsymbol{J} = \sigma\boldsymbol{E} \quad (3)$$

where σ is the electrical conductivity of the material, ϕ the electrical voltage, $\boldsymbol{E}$ the electric field vector, and $\boldsymbol{J}$ the current density vector.

2.4. Material properties

As PEF-induced pores are created, the cell becomes more permeable to electrical currents. Therefore, the electrical conductivity of the target site (myocardium) is expected to increase during pulse field delivery. The change of the electrical conductivity during PEF ablation for the myocardium can be modelled using a sigmoid function [20] dependent on the electric field magnitude $\sigma(E)$ as follows:

$$\sigma(E) = \sigma_0 + \frac{\sigma_1 - \sigma_0}{1 + 10e^{-\frac{(|E| - 58000)}{3000}}} \quad (4)$$

where σ_0 and σ_1 are the pre- and post-electroporation electric conductivities, respectively [20]. It is assumed that prior to PEF, the cell membrane is intact, so it acts as an electrical insulator. Under this condition, biological tissue behaves as in the case of low-frequency current, i.e. electrical current cannot circulate through the cytoplasm and only circulates through the extracellular space. In contrast, after PEF, the pores created in the membrane allow the passage of electric current through both the cytoplasm and the extracellular space, i.e. the cell membrane is bypassed in electrical terms, and under this condition biological tissue behaves as in the case of high-frequency current. Typically, for most animals' tissues, the transition between the low-frequency and the high-frequency behaviour occurs at a frequency band from about 10 kHz to 1 MHz [1]. While Eq. (4) was used to model the change of σ with E of myocardium affected directly by PEF energy, σ value was assumed to be constant for the other tissues (oesophagus, lungs and connective tissue) located on the opposite side of the electrodes. Specifically, we used the pre-electroporation electrical conductivity value (σ_0) because we assumed that these tissues are not electroporated since the E value should be very small in that zone. This assumption was confirmed from our

preliminary simulations, which showed identical E distributions when σ was considered constant vs. E-dependent. Interestingly, the simulation time reduces to a third when σ is constant compared to E-dependent, which confirms the high computational cost associated with solving Eq. (4) for those tissues. The electrical conductivities of the model elements are shown in Table 1 [21-23]. We initially considered the pre- and post-electroporation conductivities at 10 Hz and 500 kHz (σ_0 and σ_1), respectively. The volume of the torso surrounding the heart, the oesophagus, and the lungs was assumed to have homogeneous properties. At the level of the heart, this zone is mainly comprised of skeleton muscle and subcutaneous fat, and to a lesser extent of bony structures such as vertebrae and ribs. For this reason, we considered additional simulations in which the electrical conductivity (σ_0) of that zone was changed from connective tissue (0.251 S/m) to other tissues such as muscle tissue (skeletal) (0.202 S/m), subcutaneous fat (0.0377 S/m) and an average between these two tissues (0.12 S/m) (data from [21]).

2.5. Boundary conditions

PEF ablation setting consisted of applying a pulse of 1000 V for 100 μs in monopolar configuration, i.e. between the metal electrodes of the ablation device and the dispersive pad [5]. To model this configuration, an electrical boundary condition of ϕ = 1000 V was applied at the metal electrodes of the ablation device, while ϕ = 0 V was set at the dispersive pad surface in the case of the full torso model and at the top surface in the case of the limited-domain model (see Fig. 2). Electric current was set to be null in all the outer surfaces of the model except the surface corresponding to the dispersive pad, which implied that the electric currents flow between the metal electrodes of the ablation device and the

dispersive pad.

2.6. Sensitivity study of pre- and post-electroporation electrical conductivity

It is well known that the electrical conductivity of biological tissues increases as pulses of electroporation are applied. While an increase of approximately 300% has been observed in the case of liver tissue [24], no specific data are currently available for myocardium. Therefore, we initially chose the conductivity values at 10 Hz and 500 kHz to mimic cardiac cells pre- and post-electroporation, i.e. σ_0 = 0.0537 S/m and σ_1 = 0.281 S/m, respectively. These values correspond to a change of approximately 500%, which is certainly higher than that reported in [24]. We also conducted additional simulations considering the electrical conductivities for the myocardium at 100 Hz (σ_0 = 0.0936 S/m) and 1 MHz (σ_1 = 0.328 S/m) [21], which correspond to a change of approximately 350% and is similar to what was observed in the liver tissue. Additionally, and due to the uncertainties of electrical conductivity values for frequencies below 1 MHz where the literature values are scarce and have larger than average uncertainties [25], we considered two sets of values of myocardium electrical conductivity taken from the 'Low frequency conductivity' section of the IT'IS tissue database [21], which are more in agreement with *in vivo* experiments: the minimum and the maximum values (σ_0 = 0.1 and σ_1 = 0.775 S/m) and two intermediate values (σ_0 = 0.3 and σ_1 = 0.6 S/m). We compared the results obtained with all these conductivity values. These simulations were performed considering that the rest of the tissues (i.e. lungs, oesophagus and connective tissue) also changed their electrical conductivities as given in Table 1.

2.7. Outcome Analysis

There is limited experimental data on the electric field threshold value for PEF-induced irreversible damage in the myocardium, and moreover it is highly dependent on pulse parameters. The lowest values reported are approximately 400 V/cm [26] but values up 1000 V/cm have been recently reported [27]. While a conclusive threshold value is not currently available, we used the 400 V/cm isoline to assess and estimate 'the PEF-zone' size (maximum depth and width), as done in [12], which is similar to that used by Verma *et al* [11] in a previous computer model (550 V/cm). Since we are modelling a multi-electrode catheter aimed at creating longitudinal PEF-zones, we also quantified the total length of the PEF-zone. Note that the PEF-zone length really depends on the 'effective length' of the electrode arrangement (length of each, inter-distance and number of activated electrodes). Figure 3 shows the planes chosen to plot the electrical field distributions: 1) XY plane, which corresponds to the section plane following the axis of the catheter; and 2) YZ plane, which corresponds to the cross-sectional plane at the height of the midpoint of the third electrode (we chose the third electrode because it is around the midpoint of the 'effective length'). The maximum values of electric field in adjacent organs (oesophagus and lungs) were analysed to assess the risk of PEF ablation to damage these organs. Electrical current applied at the end of the pulse (i.e. once the impedance reached its minimum value) was also measured.

3. Results

3.1. Electric field distribution in the full torso model

Figure 4 shows the electric field distribution in the torso with connective tissue around

heart and lungs. It should be noted that the maximum values of electric field are very focused around the electrodes and that the maximum values in the adjacent organs are minimal compared to those achieved in the target zone (27 V/cm in oesophagus and 35 V/cm in lungs).

Figure 5 shows the electric field distributions around the electrodes when assuming different tissue types around the heart, oesophagus and lungs (specifically connective tissue, muscle tissue, subcutaneous fat and an average between muscle and fat). In all cases, the maximum values of electric field were very focused around the electrodes and the maximum values of electrical field in the oesophagus and lungs were much lower (16–29 V/cm in oesophagus and 30–35 V/cm in lungs). The PEF-zone size (400 V/cm isoline) was always contiguous along the catheter axis, with a length ranging from 25.79 (case of skeleton muscle, Fig. 5C) to 29.00 mm (case of subcutaneous fat, Fig. 5E). PEF-zone depth ranged from 5.98 mm (case of skeleton muscle, Fig. 5D) to 7.02 mm (case of subcutaneous fat, Fig. 5F), i.e. a maximum difference of ~1 mm. Likewise, the PEF-zone width ranged from 8.75 mm (case of skeleton muscle) to 10.57 mm (case of subcutaneous fat), i.e. a maximum difference of ~1.8 mm. The electrical current applied at the end of the electroporation ranged from 3.67 A (case of subcutaneous fat) to 6.77 A (case of connective tissue).

3.2. Sensitivity study of pre- and post-electroporation electrical conductivity

Figure 6 shows the electric field distributions around the electrodes in case of assuming different values for pre- and post-electroporation electrical conductivities (σ_0 and σ_1 respectively) considering connective tissue around the organs. We found that PEF-zone

depths were almost identical for all the cases, ranging from 6.03 mm (case of σ_0 = 0.0537 and σ_1 = 0.281 S/m, Fig. 6B) to 6.35 mm (case of σ_0 = 0.1 and σ_1 = 0.775 S/m, respectively, Fig. 6F). Likewise, the PEF-zone widths ranged from 8.98 mm (Fig. 6B) to 9.34 mm (Fig. 6F). The greatest difference was in length when comparing the cases of σ_0 = 0.1/0.3 and σ_1 = 0.6/0.775 S/m (28.67 and 28.08 mm, Fig. 6E-6G) to cases of σ_0 = 0.0537 and σ_1 = 0.281 S/m (26.22 mm, Fig. 6A) and σ_0 = 0.0936 and σ_1 = 0.328 S/m (26.77 mm, Fig. 6C). The electrical current applied at the end of the electroporation ranged from 6.77 A (case of σ_0 = 0.0537 and σ_1 = 0.281 S/m) to 7.44 A (case of σ_0 = 0.1 and σ_1 = 0.775 S/m).

3.3. Comparison between full torso and limited-domain model

Figure 7 compares the distributions of the electrical field computed from the full torso and limited-domain models. To visualize and compare the electric field distribution of both models, a XY plane of the full torso model along the ablation device up to the dispersive pad was selected as well as the XZ plane in the limited-domain model (Fig. 7A-B). Figure 7C-D corresponds with a YZ plane of the full torso model as well as the YZ plane for the limited-domain model. We found similar PEF-zone depths for both models: 6.03 mm for the torso model and 6.44 for the limited-domain model. The greatest difference was found in the PEF-zone width, where the limited-domain model predicted a value of 12.98 mm compared to 8.98 mm for the full torso model, i.e. a difference of 4 mm. Likewise the PEF-zone was longer for the limited-domain model (31.66 vs. 26.22 mm). The electrical current was slightly greater in case of full torso model: 6.77 vs. 6.45 A.

The outer dimensions of the limited-domain model were chosen to be identical to those used in previous limited-domain models for radiofrequency cardiac ablation [18]; we

conducted a sensitivity analysis to check the suitability of these values. The results showed that a 5 mm increase (i.e. X = 85 mm and Z = Y = 44 mm) hardly changed the PEF-zone size (differences of 0.05 mm in depth and 0.03 mm in width) or the current (difference of 0.04 A).

4. Discussion

Current treatment of atrial fibrillation (AF) still requires improvements in terms of safety and efficacy. Regarding efficacy, the approach of isolating the pulmonary veins involves acutely creating continuous and transmural linear lesions, which does not always ensure long term success in terms of preventing AF recurrence. Ablation of the cardiac ganglionic plexi (GP) may provide an alternative or complementary approach given the role that these neuronal cell structures play in AF initiation and maintenance [4]. Regarding safety, although recent studies suggest that endocardial pulsed electric field (PEF) ablation can reduce the possibility of damage to the oesophagus as compared to thermal techniques such as RF or cryoablation [28,29], the implications of epicardial ablation have yet to be assessed. This study addressed this issue from a computational point of view considering a novel realistic full torso model that includes the entire patient's torso and the accurate anatomy of the heart.

To our knowledge, this is the first computational model-based study for epicardial PEF ablation. Previous computer models have been proposed for endocardial PEF ablation [11,12,30]. In this regard, our results are in agreement with those previous studies which have shown the electric fields values able to provoke irreversible electroporation are possibly very focused to an area around the ablation device (see Fig. 4). Unlike previous

computational studies, we quantified the maximum values reached both in the oesophagus and lungs (<30 V/cm and <36 V/cm, respectively), confirming that the risk of damaging these organs is minimal since these values are much lower than the lethal electric field threshold for the oesophagus and lungs (1200-1500 V/cm) [31,32]. From a physical point of view, the epicardial approach tends to minimize the electric field in the oesophagus since the specific arrangement of the electrodes "points" electric power directly towards the epicardial surface, leaving the oesophagus in contact with the insulating part of the catheter.

We also found a reasonable agreement between the electrical current computed with the full torso model based on connective or muscle tissue between organs (~6.7 A) and that reported in an experimental study using the same catheter and PEF protocol (7.6±1.9 A) [5]. The difference between the experimental and computational values is possibly due to multiple factors, as suggested by the high variability reported in experiments (1.9 A). As expected, the current was lower when the organs were completely surrounded by subcutaneous fat (3.8 A) or mixed with muscle (5.8 A).

By considering the 400 V/cm isoline as an electric field threshold, our computer resulted in PEF-zone depths ranging from 5.98 and 7.02 mm. Currently, there are still very few experimental data with which to compare these computational values, and furthermore these experiments actually use a variety of pulse protocols. We also confirmed that the predicted PEF-zone depths were almost identical when the values of pre- and post-electroporation electrical conductivities (σ_0 and σ_1 respectively) were changed to be those corresponding with 100 Hz and 1 MHz and 10 Hz and 500 kHz from ‘Dielectric properties’ section of the IT’IS tissue database as well as with those corresponding with ‘Low frequency conductivity’ section of this database [21].

From the computational point of view, our results show that the limited-domain model offers qualitatively and quantitatively similar results to the full torso model (see Fig. 7), with differences of 0.41 mm in PEF-zone depth and 0.32 A in electrical current. The overestimation of PEF-zone width and length by the limited-domain model (up to 4 and 5 mm, respectively) was possibly because the geometry of the tissue surrounding the electrodes in both models is not the same: a curved shape of the heart in the full torso model (see Fig. 1B) vs. flat surface of myocardium in the limited-domain model (see Fig. 2C). Overall, these results suggest that the limited-domain model is suitable in terms of predicting PEF-zone depth and electrical current. Although certainly the reduction in the number of nodes of a domain-limited model compared to the full torso does not seem to be very relevant (from 300,000 to 110,000), especially considering that these types of models solve a stationary quasi-DC electrical problem, the limited domain model has the advantage of being based on a simpler geometry, which allows the geometric details of cardiac tissue to be modelled more realistically, as well as considering the different tissues that make up the heart wall, such as myocardium, epicardial fat, GPs, vessels, etc.

The models used in this study (both the full torso and the limited-domain models) did not consider the presence of the saline thin layer, which is typically used in ablation procedures. Saline infusion is aimed at ensuring an electrical contact between electrodes and epicardium, similar to RF tumour ablation [33]. Future studies based on limited-domain models could be used to assess the impact of the saline layer characteristics (thickness, composition, surface expansion, etc.) on the electric field distributions.

5. Conclusions

Computational results using a full torso model suggest that the electrical field is very focused around the electrodes, i.e. at the target, creating PEF-zones with depths of 6–7 mm when the lethal electric field threshold of 400 V/cm is used. The maximum values of electric field in adjacent organs (lungs and oesophagus) are much lower than the lethal electric field threshold in these organs (1200–1500 V/cm), suggesting that they are not affected by the PEF energy. The limited-domain model provided practically the same results as with the full torso model in terms of PEF-zone depth and applied current.

Declaration of Competing Interests

The authors declare no conflicts of interest.

Acknowledgments

This research was funded by Government of Ireland, Disruptive Technology Innovation Fund (DTIF), grant number DT20180123.

References

1. Sheehan MC, Srimathveeravalli G. Pulsed electric fields. Principles and Technologies for Electromagnetic Based Therapies. In Principles and Technologies for Electromagnetic Energy Based Therapies. Prakash P, Srimathveeravalli G (Eds.). Elsevier Academic Press. 2021. ISBN: 9780128205945, pp: 71-106.
2. Sugrue A, Vaidya V, Witt C, DeSimone CV, Yasin O, Maor E, Killu AM, Kapa S, McLeod CJ, Miklavčič D, Asirvatham SJ. Irreversible electroporation for catheter-based cardiac ablation: a systematic review of the preclinical experience. J Interv Card Electrophysiol. 2019 Sep;55(3):251-265. doi: 10.1007/s10840-019-00574-3.
3. Wittkampf FHM, van Es R, Neven K. Electroporation and its Relevance for Cardiac Catheter Ablation. JACC Clin Electrophysiol. 2018 Aug;4(8):977-986. doi: 10.1016/j.jacep.2018.06.005.
4. Patterson E, Po SS, Scherlag BJ, Lazzara R. Triggered firing in pulmonary veins initiated by in vitro autonomic nerve stimulation. Heart Rhythm. 2005 Jun;2(6):624-31. doi: 10.1016/j.hrthm.2005.02.012.
5. Padmanabhan D, Naksuk N, Killu AK, Kapa S, Witt C, Sugrue A, DeSimone CV, Madhavan M, de Groot JR, O'Brien B, Rabbette T, Coffey K, Asirvatham SJ. Electroporation of epicardial autonomic ganglia: Safety and efficacy in medium-term canine models. J Cardiovasc Electrophysiol. 2019 Apr;30(4):607-615. doi: 10.1111/jce.13860.
6. Madhavan M, Venkatachalam KL, Swale MJ, Desimone CV, Gard JJ, Johnson SB, Suddendorf SH, Mikell SB, Ladewig DJ, Nosbush TG, Danielsen AJ, Knudson M, Asirvatham SJ. Novel Percutaneous Epicardial Autonomic Modulation in the Canine for Atrial Fibrillation: Results of an Efficacy and Safety Study. Pacing Clin Electrophysiol. 2016 May;39(5):407-17. doi: 10.1111/pace.12824.
7. Avazzadeh S, McBride S, O'Brien B, Coffey K, Elahi A, O'Halloran M, Soo A, Quinlan LR. Ganglionated Plexi Ablation for the Treatment of Atrial Fibrillation. J Clin Med. 2020 Sep 24;9(10):3081. doi: 10.3390/jcm9103081.
8. Iasiello M, Andreozzi A, Bianco N, Vafai K. The porous media theory applied to radiofrequency catheter ablation. Int J Numerical Methods for Heat & Fluid Flow. 2020;30(5):2669-2681. doi:10.1108/HFF-11-2018-0707.
9. González-Suárez A, Berjano E. Comparative analysis of different methods of modeling the thermal effect of circulating blood flow during RF cardiac ablation. IEEE Transactions on Biomedical Engineering 2015, 63(2), 250-259.
10. Aycock KN, et al. Experimental and numerical investigation of parameters affecting high-frequency irreversible electroporation for prostate cancer ablation. J Biomech Eng. 2022 Jan 19. doi: 10.1115/1.4053595.
11. Verma A, Asivatham SJ, Deneke T, Castellvi Q, Neal RE 2nd. Primer on Pulsed Electrical Field Ablation: Understanding the Benefits and Limitations. Circ Arrhythm Electrophysiol. 2021 Sep;14(9):e010086. doi: 10.1161/CIRCEP.121.010086.
12. Stewart MT, Haines DE, Miklavčič D, Kos B, Kirchhof N, Barka N, Mattison L, Martien M, Onal B, Howard B, Verma A. Safety and chronic lesion characterization of pulsed field ablation in a Porcine model. J Cardiovasc Electrophysiol. 2021 Apr;32(4):958-969. doi: 10.1111/jce.14980.
13. Gosselin MC, Neufeld E, Moser H, Huber E, Farcito S, Gerber L, Jedensjö M, Hilber I, Di Gennaro F, Lloyd B, Cherubini E, Szczerba D, Kainz W, Kuster N. Development of a new generation of high-resolution anatomical models for medical device evaluation: the Virtual Population 3.0. Phys Med Biol. 2014;59(18):5287-303.
14. Cignoni P, Callieri M, Corsini M, Dellepiane M, Ganovelli F, Ranzuglia G. MeshLab: an open-source mesh processing tool. Eurographics Italian Chapter Conference. 2008, 129-136. Scarano V, De Chiara R and Erra U (Editors).
15. Geuzaine C, Remacle JF. Gmsh: a three-dimensional finite element mesh generator with built-in pre- and post-processing facilities. Int J Numer Meth Eng. 2009;79(11):1309–1331.
16. Marchandise E, Compère G, Willemet M, Bricteux G, Geuzaine C, Remacle JF. Quality meshing based on stl triangulations for biomedical simulations. Int J Numer Method Biomed Eng. 2010, 26(7): 876-889. doi: 10.1002/cnm.1388.
17. Berjano EJ and Hornero F. A cooled intraesophageal ballon to prevent thermal injury during endocardial surgical radiofrequency ablation of the left atrium: a finite element study. Phys Med Biol. 2005; 50:N69-N279

18. Irastorza RM, Gonzalez-Suarez A, Pérez JJ, Berjano E. Differences in applied electrical power between full thorax models and limited-domain models for RF cardiac ablation. Int J Hyperthermia 2020;37(1):677-687.
19. Trujillo M, Castellví Q, Burdío F, Sánchez-Velázquez P, Ivorra A, Andaluz A, Berjano E. Can electroporation previous to radiofrequency hepatic ablation enlarge thermal lesion size? A feasibility study based on theoretical modelling and in vivo experiments. Int J Hyperthermia. 2013;29(3):211-218.
20. Sel D, Cukjati D, Batiuskaite D, Slivnik T, Mir LM, Miklavcic D. Sequential finite element model of tissue electropermeabilization. IEEE Trans Biomed Eng. 2005;52(5):816-27
21. Hasgall PA, Di Gennaro F, Baumgartner C, et al. IT'IS Database for thermal and electromagnetic parameters of biological tissues, Version 3.0. [2015 Sep 01], Available from: www.itis.ethz.ch/database.
22. Pérez JJ, Ewertowska E, Berjano E. Computer modeling for radiofrequency bipolar ablation inside ducts and vessels: relation between pullback speed and impedance progress. Lasers Surg Med. 2020 Nov;52(9):897-906. doi: 10.1002/lsm.23230.
23. Berjano EJ, Hornero F. What affects esophageal injury during radiofrequency ablation of the left atrium? An engineering study based on finite-element analysis. Physiol Meas. 2005 Oct;26(5):837-48. doi: 10.1088/0967-3334/26/5/020.
24. Ivorra A, Rubinsky B. In vivo electrical impedance measurements during and after electroporation of rat liver. Bioelectrochemistry. 2007 May;70(2):287-95. doi: 10.1016/j.bioelechem.2006.10.005.
25. Gabriel C, Peyman A, Grant EH. Electrical conductivity of tissue at frequencies below 1 MHz. Phys Med Biol. 2009 Aug 21;54(16):4863-78. doi: 10.1088/0031-9155/54/16/002.
26. Kaminska I, Kotulska M, Stecka A, Saczko J, Drag-Zalesinska M, Wysocka T, Choromanska A, Skolucka N, Nowicki R, Marczak J, Kulbacka J. Electroporation-induced changes in normal immature rat myoblasts (H9C2). Gen Physiol Biophys. 2012 Mar;31(1):19-25. doi: 10.4149/gpb_2012_003.
27. Avazzadeh S, O'Brien B, Coffey K, O'Halloran M, Keane D, Quinlan LR. Establishing irreversible electroporation electric field potential threshold in a suspension in vitro model for cardiac and neuronal cells. J Clin Med. 2021; 10(22):5443.
28. Cochet H, Nakatani Y, Sridi-Cheniti S, Cheniti G, Ramirez FD, Nakashima T, Eggert C, Schneider C, Viswanathan R, Derval N, Duchateau J, Pambrun T, Chauvel R, Reddy VY, Montaudon M, Laurent F, Sacher F, Hocini M, Haïssaguerre M, Jais P. Pulsed field ablation selectively spares the oesophagus during pulmonary vein isolation for atrial fibrillation. Europace. 2021 Sep 8;23(9):1391-1399. doi: 10.1093/europace/euab090.
29. Howard B, Haines DE, Verma A, Packer D, Kirchhof N, Barka N, Onal B, Fraasch S, Miklavčič D, Stewart MT. Reduction in Pulmonary Vein Stenosis and Collateral Damage With Pulsed Field Ablation Compared With Radiofrequency Ablation in a Canine Model. Circ Arrhythm Electrophysiol. 2020 Sep;13(9):e008337. doi: 10.1161/CIRCEP.120.008337.
30. Ramirez FD, Reddy VY, Viswanathan R, Hocini M, Jaïs P. Emerging Technologies for Pulmonary Vein Isolation. Circ Res. 2020 Jun 19;127(1):170-183. doi: 10.1161/CIRCRESAHA.120.316402.
31. Satkauskas S, Batiuskaite D, Salomskaite-Davalgiene S, Venslauskas MS. Effectiveness of tumor electrochemotherapy as a function of electric pulse strength and duration. Bioelectrochemistry 2005 Feb;65(2):105-11.doi: 10.1016/j.bioelechem.2004.08.003.
32. Song Y, Zheng J , Fan L. Nonthermal Irreversible Electroporation to the Esophagus: Evaluation of Acute and Long-Term Pathological Effects in a Rabbit Model. J Am Heart Assoc 2021 Nov 16;10(22):e020731.doi: 10.1161/JAHA.120.020731.
33. Leveillee RJ, Hoey MF, Hulbert JC, Mulier P, Lee D, Jesserun J. Enhanced radiofrequency ablation of canine prostate utilizing a liquid conductor: the virtual electrode. J Endourol. 1996 Feb;10(1):5-11. doi: 10.1089/end.1996.10.5.

Table 1. Electrical conductivity (σ) of the elements used in the computational models: electrode, insulation, heart, saline, oesophagus, lung, torso and saliva. σ_0 and σ_1 correspond to the pre- and post-electroporation electrical conductivity values, respectively. Data from [21-23].

Element/Material	**Case 1**		**Case 2**		**Case 3**	
	σ_0 (S/m)	**σ_1 (S/m)**	**σ_0 (S/m)**	**σ_1 (S/m)**	**σ_0 (S/m)**	**σ_1 (S/m)**
Electrode/Stainless steel	4.6×10^{6}					
Insulation/Polyurethane	10^{-5}					
Heart/Myocardium	0.0537	0.281	0.0936	0.328	0.1/0.3	0.6/0.775
Oesophagus*	0.511		0.522		0.164	
Lung (deflated)*	0.203		0.206		0.111	
Torso/Connective tissue*	0.251		0.305		0.0792	
Saliva	1.2					

*The value of electrical conductivity of these tissues was set at pre-electroporation conductivity value (σ_0) since they are not electroporated (the E value is very low in comparison to their irreversible electroporation threshold which is in the range from 1200 to 1500 V/cm [31-32]).

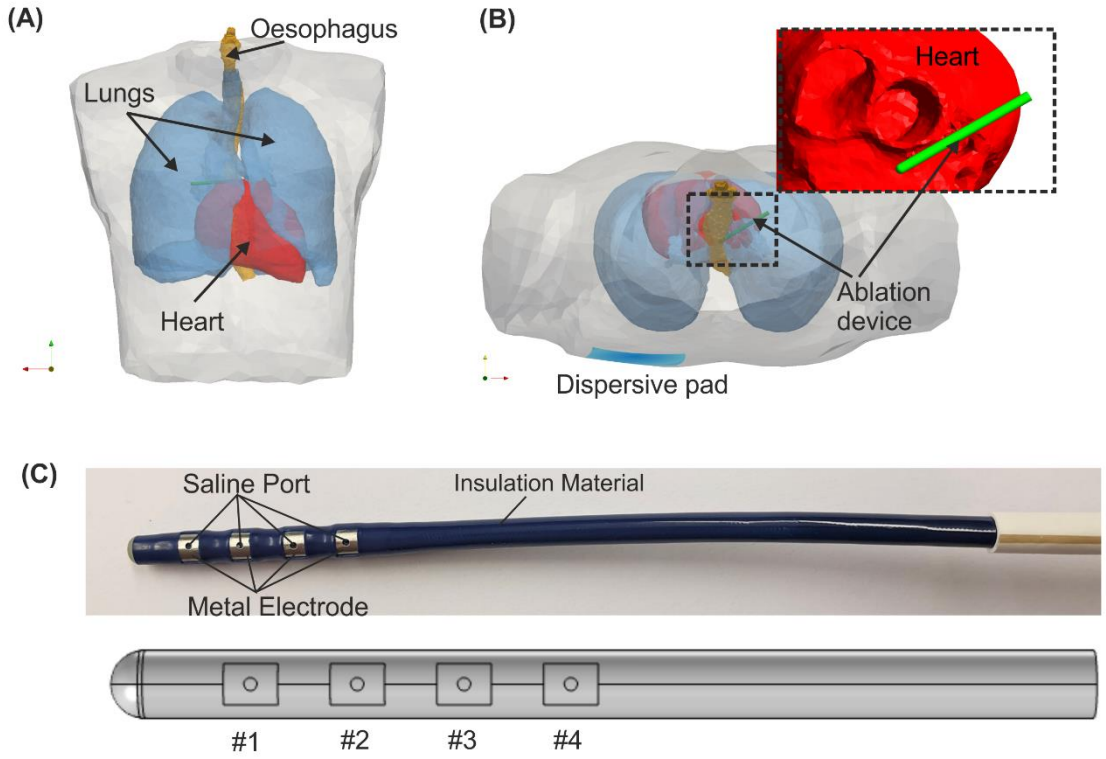

Figure 1 **A:** Geometry of the 3D model based on the real anatomy of the torso, including oesophagus and lungs. The dispersive pad is located at the patient's back. **B:** Detail of the ablation device on the epicardium. **C:** Ablation catheter (AtriAN Medical, Galway, Ireland) which comprises four metal electrodes with a hole in their centre for saline infusion, and an insulating part between the metal electrodes.

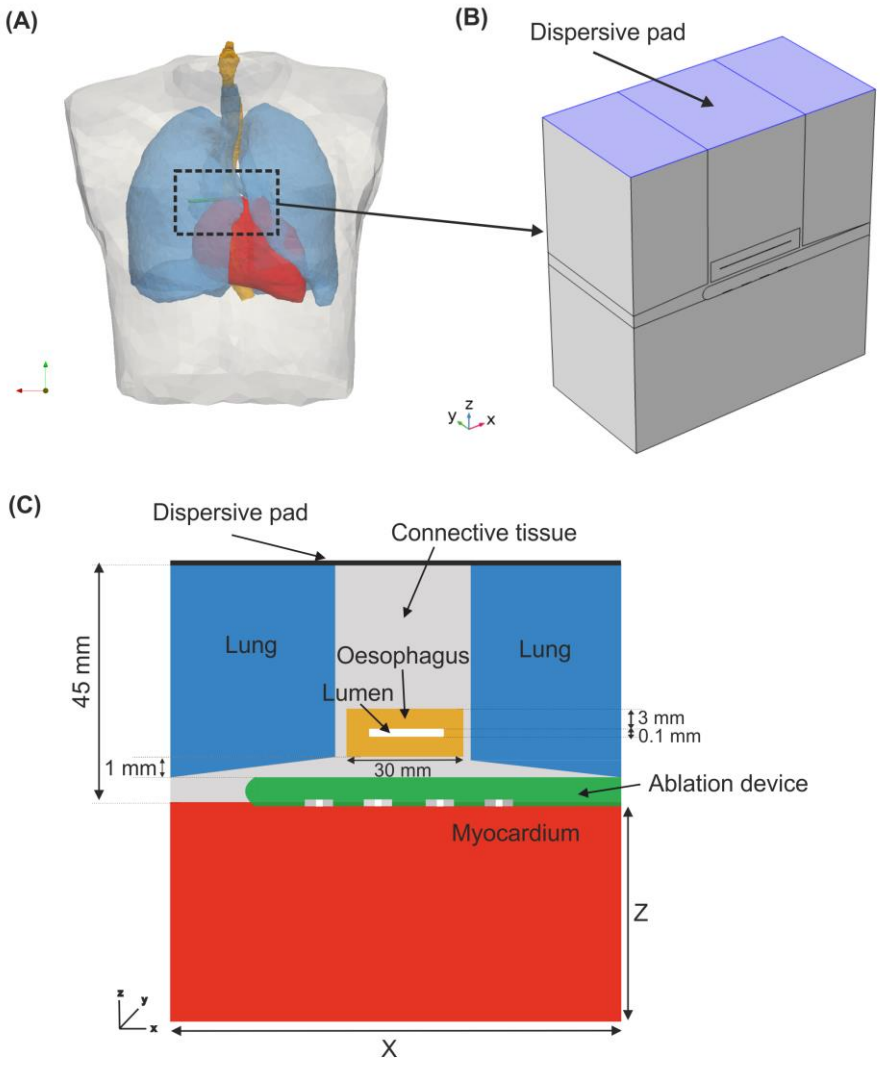

Figure 2 Geometry of the 3D limited-domain model (**B**) which only considers a fragment of the region of interest corresponding with the full torso (**A**). The dispersive pad in the limited-domain model is placed on the top surface of the model (**B** and **C**).

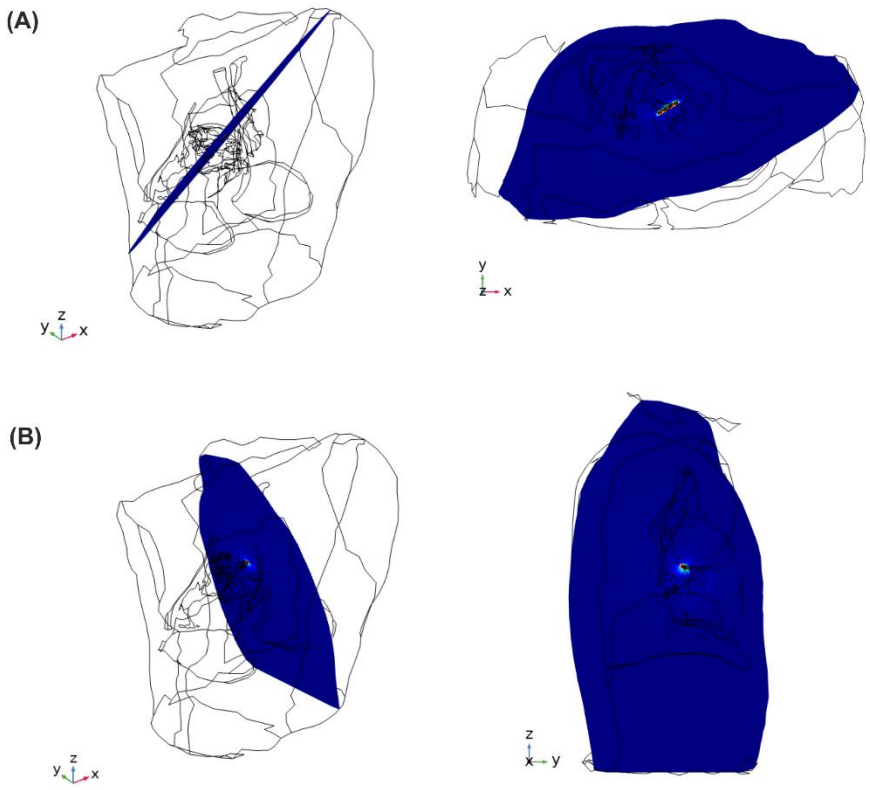

Figure 3 Planes chosen to plot the electrical field distributions: **(A)** The XY plane corresponds with the section plane following the axis of the catheter; **(B)** The YZ plane corresponds with the cross-sectional plane at the height of the midpoint of the third electrode.

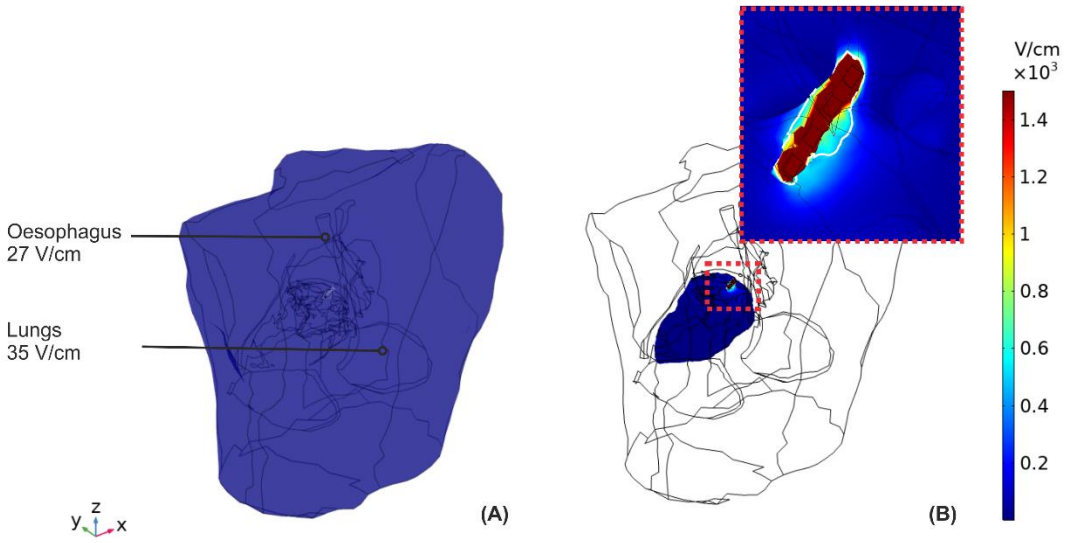

Figure 4 Electric field distribution in the full torso model (**A**) and detail of around the ablation electrodes (**B**). Note that the maximum values of electric field in adjacent organs (oesophagus and lungs) is lower than their irreversible electroporation threshold which is in the range from 1200 to 1500 V/cm [31-32]. This figure corresponds to the case in which the organs (heart, lungs and oesophagus) are surrounded by connective tissue. The white contour corresponds to the 400 V/cm electric field isoline.

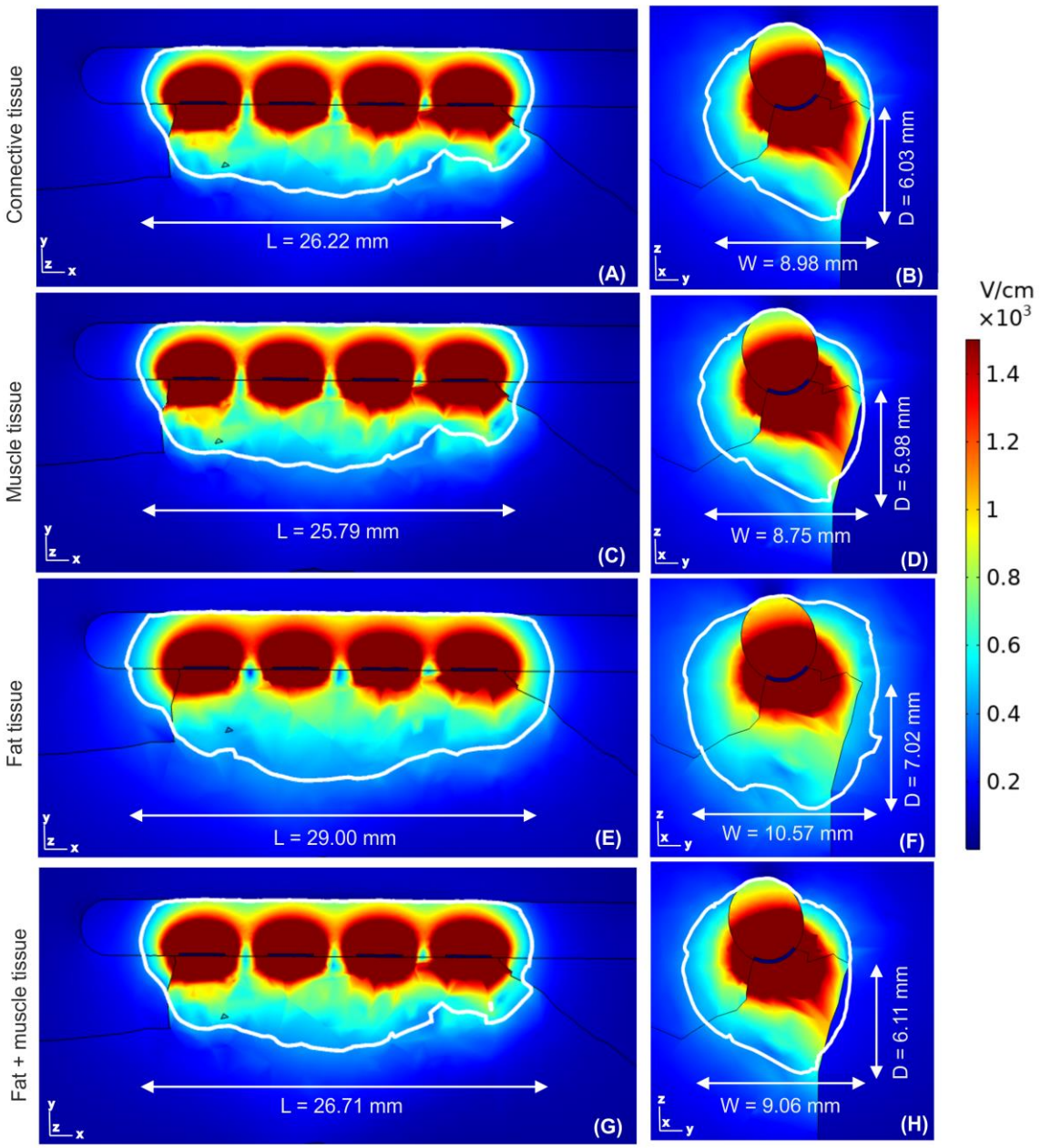

Figure 5 Electric field distributions around the electrodes corresponding with the longitudinal axis (**A,C,E,G**) and transverse through the middle point of the third electrode (**B,D,F,H**) for different types of tissue surrounding the organs: connective (**A,B**), muscle (**C,D**), fat (**E,F**) and mixture of fat and muscle (**G,H**). The white contour corresponds to the 400 V/cm electric field isoline.

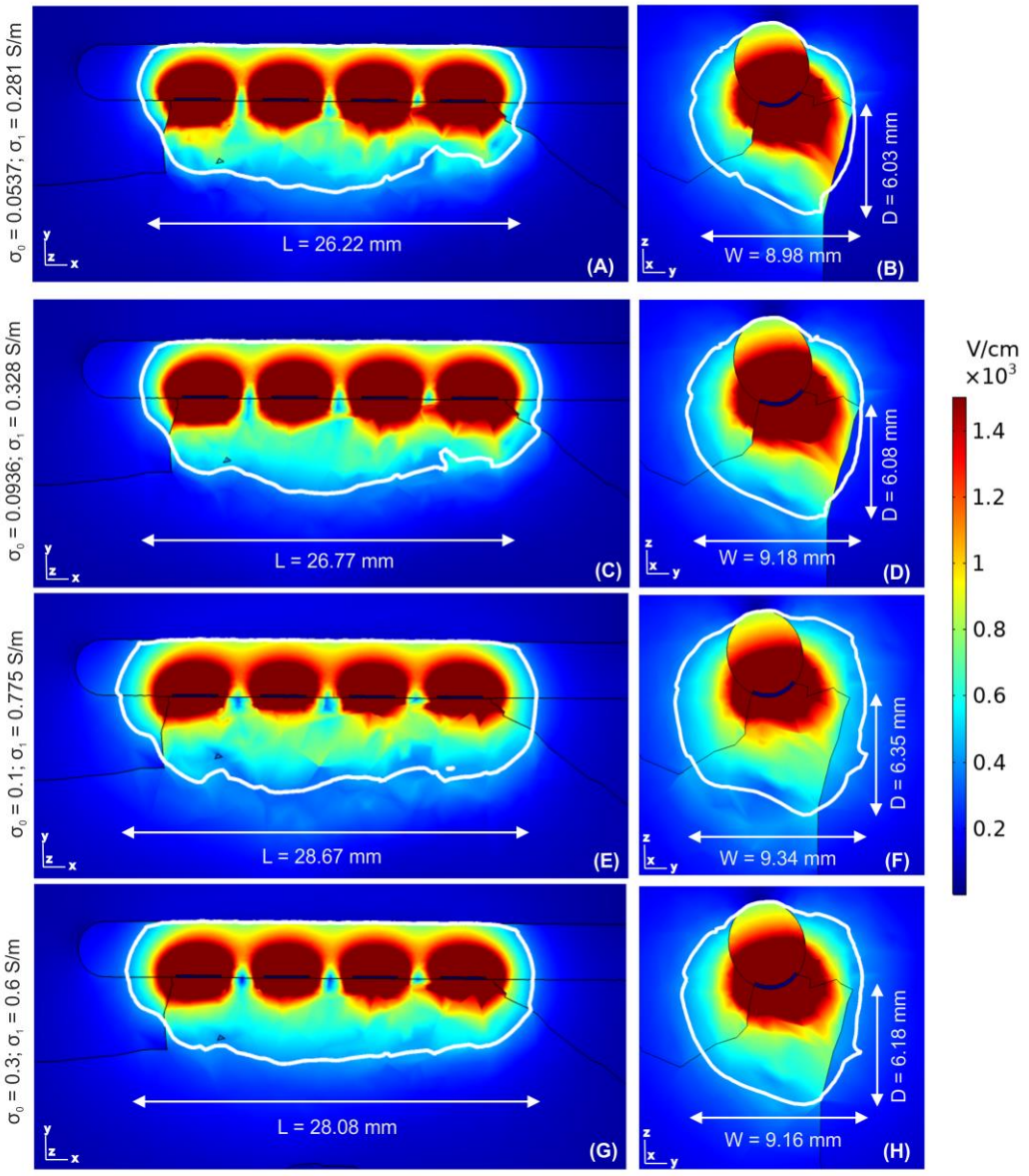

Figure 6 Electric field distributions on planes XY **(A,C,E,G)** and YZ **(B,D,F,H)** around the electrodes in case of assuming different values for pre- and post-electroporation electrical conductivities (σ_0 and σ_1) for the myocardium, specifically σ_0 = 0.037 S/m and σ_1 = 0.281 S/m **(A,B)**, σ_0 = 0.0936 S/m and σ_1 = 0.328 S/m **(C,D)**, σ_0 = 0.1 S/m and σ_1 = 0.775 S/m **(E,F)** and σ_0 = 0.3 S/m and σ_1 = 0.6 **(G,H)**. The simulations correspond to the case of connective tissue around the organs. The white contour corresponds to the 400 V/cm electric field isoline.

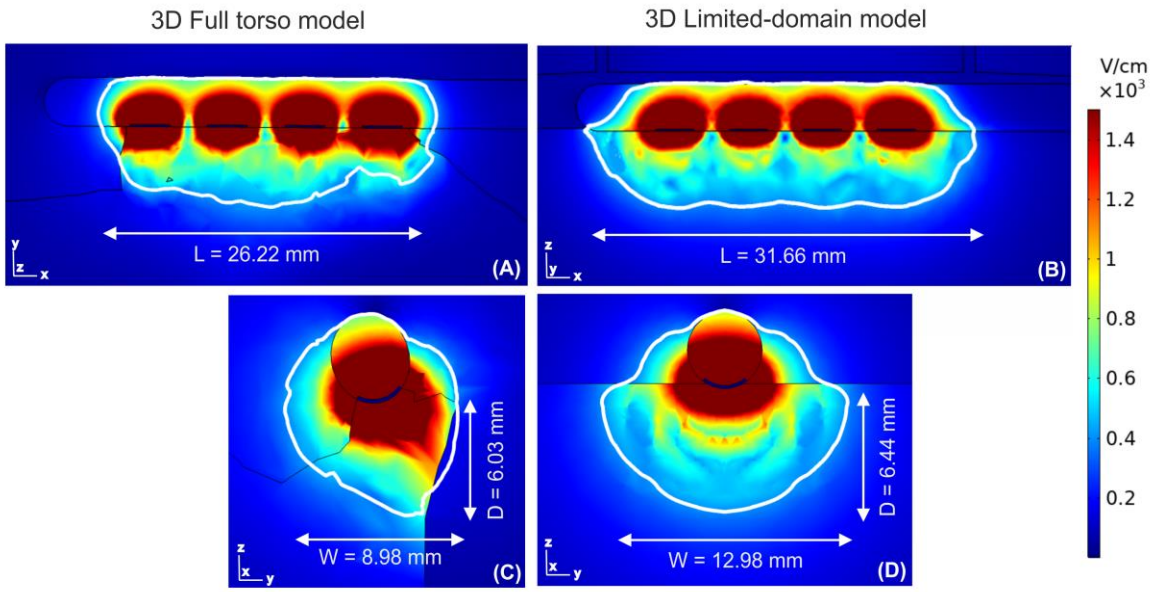

Figure 7 Electric field distributions on planes XY **(A,B)** and YZ **(C,D)** around the electrodes computed from the 3D full torso (**A,C**) and the 3D limited-domain model (**B,D**) (both with the same scale). The white contour corresponds to the 400 V/cm electric field isoline.